




# Antemortem volume loss mirrors TDP-43 staging in older adults with non-frontotemporal lobar degeneration

 Alexandre Bejanin,<sup>1,2</sup> Melissa E. Murray,<sup>3</sup> Peter Martin,<sup>4</sup>  Hugo Botha,<sup>1</sup> Nirubol Tosakulwong,<sup>4</sup> Christopher G. Schwarz,<sup>5</sup> Matthew L. Senjem,<sup>5,6</sup> Gael Chételat,<sup>2</sup> Kejal Kantarci,<sup>5</sup> Clifford R. Jack, Jr,<sup>5</sup> Bradley F. Boeve,<sup>1</sup> David S. Knopman,<sup>1</sup> Ronald C. Petersen,<sup>1</sup> Caterina Giannini,<sup>7</sup> Joseph E. Parisi,<sup>7</sup>  Dennis W. Dickson,<sup>3</sup> Jennifer L. Whitwell<sup>5</sup> and Keith A. Josephs<sup>1</sup>

Over the past decade, the transactive response DNA-binding protein of 43 kDa (TDP-43) has been recognized as a major protein in normal and pathological ageing, increasing the risk of cognitive impairment and dementia. In conditions distinct from the frontotemporal lobar degenerations, TDP-43 appears to progress in a stereotypical pattern. In the present study, we aimed at providing a better understanding of the effects of TDP-43 and other age-related neuropathologies on cross-sectional grey matter volume in a cohort of non-FTLD subjects. We included 407 individuals with an antemortem MRI and post-mortem brain tissue from the Mayo Clinic Alzheimer's Disease Research Center, Mayo Clinic Alzheimer's Disease Patient Registry, or the Mayo Clinic Study of Aging. All individuals were assigned pathological stages for TDP-43, tau, amyloid- $\beta$ , Lewy bodies, argyrophilic grain disease and vascular pathologies. Robust regressions were performed in regions of interest and voxel-wise to explore the relationships between TDP-43 stages and grey matter volume while controlling for other pathologies. Grey matter volumes adjusted for pathological and demographic variables were also computed for each TDP-43-positive case to further characterize the sequential involvement of brain structures associated with TDP-43, irrespective of the TDP-43 staging scheme. Robust regressions showed that the extent of TDP-43 pathology was associated with the extent of grey matter atrophy. Specifically, we found that the volume in medial temporal regions (i.e. amygdala, entorhinal cortex, hippocampus) decreased progressively with advancing TDP-43 stages. Importantly, these effects were of similar magnitude to those related to tau stages. Additional analyses using adjusted grey matter volume demonstrated a sequential pattern of volume loss associated with TDP-43, starting within the medial temporal lobe, followed by early involvement of the temporal pole, and eventually encompassing additional temporal and frontal regions. Altogether, this study demonstrates the major and independent contribution of TDP-43 pathology on neurodegeneration and provides further insight into the regional distribution of TDP-43 in non-FTLD subjects. Along with previous studies, these findings emphasized the importance of targeting TDP-43 in future clinical trials to prevent its detrimental effect on grey matter volume and, eventually, cognition.

1 Department of Neurology, Mayo Clinic, Rochester, MN, USA

2 Inserm, Inserm UMR-S U1237, Université de Caen-Normandie, GIP Cyceron, Caen, France

3 Department of Neuroscience, Mayo Clinic, Florida, USA

4 Health Science Research, Mayo Clinic, Rochester, MN, USA

5 Department of Radiology, Mayo Clinic, Rochester, MN, USA

6 Department of Information Technology, Mayo Clinic, Rochester, MN, USA

7 Department of Laboratory Medicine and Pathology, Mayo Clinic, Rochester, MN, USA

Correspondence to: Alexandre Bejanin  
 Department of Neurology, Mayo Clinic, Rochester, MN, USA  
 E-mail: bejanin.cyceron@gmail.com

**Keywords:** TDP-43; tau;  $\beta$ -amyloid; radiological-pathological study; neuropathology

**Abbreviations:** FTLD = frontotemporal lobar degeneration; MCALT = Mayo Clinic Adult Lifespan Template; TDP-43 = transactive response DNA-binding protein of 43 kDa

## Introduction

In 2006, the pathological transactive response DNA-binding protein of 43 kDa (TDP-43) was shown to be the major disease protein in amyotrophic lateral sclerosis and in frontotemporal lobar degeneration (FTLD) with ubiquitin-positive inclusions (Arai *et al.*, 2006; Neumann *et al.*, 2006). Subsequently, TDP-43 was found to be present in the brains of patients with Alzheimer's disease (Amador-Ortiz *et al.*, 2007; Higashi *et al.*, 2007) and other neurodegenerative diseases such as Lewy body disease (Higashi *et al.*, 2007; Nakashima-Yasuda *et al.*, 2007), hippocampal sclerosis (Amador-Ortiz *et al.*, 2007) or argyrophilic grain disease (Fujishiro *et al.*, 2009). Additionally, ~20% of older adults with normal cognition and low Alzheimer's disease neuropathology present with TDP-43 inclusions (for meta-analysis, see Nascimento *et al.*, 2018).

Across these conditions, TDP-43 appears to develop in a stereotypical pattern (Hu *et al.*, 2008; Josephs *et al.*, 2014a, 2016; Nag *et al.*, 2015, 2018; Tan *et al.*, 2015). Indeed, TDP-43 inclusions are first deposited in the amygdala, followed by the entorhinal cortex and hippocampus, and then neocortical regions in Alzheimer's disease (Hu *et al.*, 2008; Josephs *et al.*, 2014a) or primary age-related tauopathy (Josephs *et al.*, 2017b, 2019b; Zhang *et al.*, 2019), and Lewy body disease (Arai *et al.*, 2009; Yokota *et al.*, 2010). The topography of TDP-43 inclusions was further shown to follow a six-stage scheme in Alzheimer's disease that starts in the amygdala (stage 1), followed by the subicular region of the hippocampus and/or entorhinal cortex (stage 2), the dentate gyrus of the hippocampus and/or occipitotemporal cortex (stage 3), the ventral striatum, basal forebrain, insular and/or inferior temporal cortex (stage 4), the substantia nigra, inferior olive and/or midbrain tectum (stage 5), and finally the middle frontal cortex and/or basal ganglia (stage 6) (Josephs *et al.*, 2016). This staging was also used to characterize the regional distribution of TDP-43 pathology in older adults with normal cognition or Lewy body dementia (McAleese *et al.*, 2017), and in cases with primary age-related tauopathy (Josephs *et al.*, 2017b, 2019b).

The relevance of this pathological staging scheme was emphasized by associations with clinical features (Josephs *et al.*, 2014a, 2016) but little is known about the relations with antemortem brain structure. Previous studies reported that the presence of TDP-43 pathology is associated with medial temporal lobe atrophy in Alzheimer's disease

(Josephs *et al.*, 2008a, 2014b, 2015) and in heterogeneous pathological cohorts (Kovacs *et al.*, 2013; Hanko *et al.*, 2018). With increasing TDP-43 stages, individuals with Alzheimer's disease have more atrophy in the entorhinal cortex and hippocampus (Josephs *et al.*, 2014a). Furthermore, TDP-43 in and beyond the hippocampus (stage  $\geq 2$ ) was found to increase the longitudinal rate of hippocampal atrophy in Alzheimer's disease (Josephs *et al.*, 2017a). Yet, the relative effect of TDP-43 staging compared to other age-related neuropathologies is still unclear in more heterogeneous populations.

The main objective of this cross-sectional study was therefore to provide a better understanding of the topography of grey matter loss associated with TDP-43 inclusions in a large cohort ( $n = 407$ ) of older adults without FTLD. Specifically, we first assessed the effect of the regional distribution of TDP-43 pathology on antemortem grey matter volumes. To do so, we used robust regressions to explore the pattern of grey matter atrophy related to TDP-43 stages while controlling for other pathological variables such as tau (i.e. Braak stage), amyloid- $\beta$  (i.e. diffuse and neuritic plaques), Lewy bodies, argyrophilic grain disease and vascular pathologies. We then computed grey matter volumes adjusted for pathological (except TDP-43) and demographic variables to further determine the sequential involvement of brain structures in TDP-43-positive cases, irrespective of their TDP-43 stage. This latter approach was aimed at better describing the volume loss related to TDP-43 while compensating for some limitations of pathological examinations, such as the fact that only one hemisphere is usually screened and only a limited number of brain regions are assessed.

## Materials and methods

### Participants

For the present study, we identified all individuals who had (i) been prospectively followed up in the Mayo Clinic Alzheimer's Disease Research Center (ADRC), Mayo Clinic Alzheimer's Disease Patient Registry (ADPR), or the Mayo Clinic Study of Aging (MCSA); (ii) had died with a brain autopsy; (iii) had one usable antemortem volumetric MRI scan acquired after 1 January 1999; and (iv) had a complete set of available paraffin blocks of brain tissue for TDP-43, tau, amyloid and Lewy body analysis. Individuals with a pathological diagnosis of FTLD or primary tauopathies were

excluded. Specifically, individuals were excluded if they had unequivocal evidence of focal frontal or temporal lobe neuronal loss or gliosis and met published criteria for FTL (Cairns *et al.*, 2007). The Mayo Clinic ADRC recruits patients with mild cognitive impairment or dementia from the Department of Neurology, Mayo Clinic. The ADRC is a community-based study of cognitive ageing, while the MCSA is a prospective population-based study of cognitive ageing (Roberts *et al.*, 2008), with both studies recruiting from Olmsted County, Minnesota. For each participant, determination of cognitively unimpaired status was based on consensus agreement between the study coordinator, examining physician, and neuropsychologist who evaluated the participant, taking into account education, prior occupation, visual or hearing deficits, and other available clinical information. All participants underwent apolipoprotein E (*APOE*) genotyping. This study was approved by the Mayo Clinic Institutional Review Board. Before death, all participants or their proxies provided written consent for brain autopsy examination.

## Pathological examination

All individuals underwent a pathological examination according to the recommendations of the Consortium to Establish a Registry for Alzheimer's disease (CERAD) (Mirra *et al.*, 1991). Each individual was assigned a Braak neurofibrillary tangle stage (Braak and Braak, 1991), a Lewy body stage [0: no Lewy body pathology, 1: brainstem predominant, 2: limbic (transitional), 3: neocortical (diffuse), 4: amygdala predominant] (Montine *et al.*, 2012), a score for neuritic amyloid- $\beta$  plaques (0: none, 1: sparse neuritic plaques, 2: moderate neuritic plaques, 3: frequent neuritic plaques) (Mirra *et al.*, 1991), diffuse amyloid- $\beta$  plaques (0: none, 1: sparse diffuse plaques, 2: moderate diffuse plaques, 3: frequent diffuse plaques), argyrophilic grain disease (0: absent, 1: present) and vascular pathology (0: no vascular infarcts, 1: microinfarcts or lacunar/large infarcts, 2: both microinfarcts and lacunar/larger infarcts) (Wennberg *et al.*, 2019). Note that given the small number of individuals at Braak stages 0 and I, these stages were pooled together with Braak stage II to better estimate the effects of more advanced Braak stages.

In addition, all individuals were assessed for the presence of TDP-43 independent of TDP-43 type (Josephs *et al.*, 2019c) in the amygdala as previously described (Josephs *et al.*, 2016). For all individuals in whom TDP-43 was observed in the amygdala, the presence of TDP-43 was subsequently assessed in 13 additional brain regions: entorhinal cortex, subiculum, dentate gyrus of the hippocampus, occipitotemporal cortex, insula, ventral striatum, basal forebrain, inferior temporal, substantia nigra, inferior olive, midbrain tectum, basal ganglia, and middle frontal. A region was considered TDP-43-positive if there were any TDP-43 immunoreactive neuronal cytoplasmic inclusions, dystrophic neurites, neuronal intranuclear inclusions or neurofibrillary tangle-associated TDP-43 identified at  $\times 400$  magnification. Following previous criteria (Josephs *et al.*, 2016), all individuals were staged with the following rule: only one region from a specific stage needs to be involved in order to attain that stage, and the highest region involved determines the stage (for further details and the specific involvement of the inferior olive, see Josephs *et al.*, 2016). Cases were classified as follows: TDP-43-negative (no inclusion in the amygdala), TDP-43 stage 1 (amygdala only), TDP-43 stage 2

(entorhinal cortex and/or subiculum), TDP-43 stage 3 (dentate gyrus of the hippocampus and/or occipitotemporal cortex) and TDP-43 stage 4+ (inclusions beyond the medial temporal lobe, i.e. brain regions associated with stage 4–6). We included only individuals for whom TDP-43 was screened in at least one brain region of each stage above their own stage (e.g. a subject at stage 2 was included if the presence of TDP-43 was assessed in at least one region of stage 3 and one region of stage 4+). This way, we avoided underestimating the stage of an individual. It is also worth mentioning that (i) TDP-43 was assessed for all TDP-43-positive cases in the amygdala, entorhinal cortex, subiculum and dentate gyrus of the hippocampus, and middle frontal gyrus; (ii) >97% of the cases were screened in the occipitotemporal cortex, insula, basal forebrain, midbrain tectum, and basal ganglia; and (iii) all TDP-43 stage regions were assessed in 102 TDP-43-positive cases.

## Neuroimaging data

The MRI closest to death was selected for each subject to correspond to the pathological data (time delay between MRI and death =  $3.6 \pm 2.4$  years). All MRI scans were done with a standardized protocol that included a  $T_1$ -weighted 3D volumetric sequence. Subjects were either scanned at 1.5 T ( $n = 239$ ) or 3 T ( $n = 168$ ), and the MRI field strength was included as a covariate in all analyses. All images underwent corrections for gradient non-linearity (Jovicich *et al.*, 2006), and were corrected for intensity inhomogeneity, segmented and normalized to the Mayo Clinic Adult Lifespan Template (MCALT) (Schwarz *et al.*, 2017) (<https://www.nitrc.org/projects/mcalt/>) using the SPM12 Unified Segmentation (Ashburner and Friston, 2005) with MCALT priors and settings. Grey matter probability maps were then smoothed using a 6 mm full-width at half-maximum Gaussian kernel. Grey matter volumes for specific regions of interest were computed using MCALT atlases. Normalization parameters were computed between each image and the MCALT template using ANTs software (Avants *et al.*, 2008) and the MCALT atlases were propagated to native image space and used to compute the regional values. Finally, raw and preprocessed images were checked visually to assess data quality, and 16 cases were excluded because of acquisition or segmentation issues.

## Statistical analyses

The relationships between pathological TDP-43 staging and antemortem grey matter volumes were assessed using robust regressions (robustbase package) (Maechler *et al.*, 2018) in R (R Core Team, 2014). Robust methods are particularly useful when a large number of regressions are tested and assumptions cannot be evaluated for each individual regression. Furthermore, robust regressions are relatively insensitive to the presence of one or more outliers in the data and provide more accurate coefficients. Analyses were performed in regions of interest that match those screened for the presence of TDP-43: amygdala (stage 1), entorhinal cortex and hippocampus (stages 2 and 2–3, respectively), fusiform gyrus (stage 3), insula, inferior temporal and middle frontal gyri (stage 4+). Robust regressions were performed using the volume of each region of interest as the dependent variable and the TDP-staging (five levels: 0, 1, 2, 3, 4+) as the independent variable. Statistical models were adjusted for the other pathological

variables: Braak stage (five levels: 0–II, III, IV, V, VI), Lewy body stage (five levels: 0, 1, 2, 3, 4), neuritic (continuous) and diffuse (continuous) amyloid- $\beta$  plaques, argyrophilic grain disease (two levels: 0, 1) and vascular pathology (continuous). The time delay between MRI and death (continuous), age at MRI (continuous), sex (two levels: male, female), total intracranial volume (continuous) and MRI field strength (two levels: 1.5 T, 3 T) were also regressed out in all models. The same analysis was then performed voxel-wise using the *oro-nifti* (Whitcher *et al.*, 2011) package to import nifti files. Voxel-wise analyses were performed in a mask excluding non-grey matter voxels. To correct for multiple comparisons, we used thresholds of false discovery rate (FDR)-corrected  $P < 0.001$  and cluster extent  $k > 500 \text{ mm}^3$  for voxel-wise analyses (using the *fdr* function implemented in FSL-5.0.10), and Bonferroni-corrected  $P < 0.05$  for region of interest analyses. To detect more subtle effects, voxel-wise results were additionally presented at an uncorrected threshold of  $P < 0.001$  ( $k > 500 \text{ mm}^3$ ). Finally, volume was log-transformed in all analyses so that estimated change could be interpreted on a percentage scale. Results for pathological staging are presented in comparison to the group with no or low pathology (e.g. TDP-43-negative, Braak stage 0–II, and Lewy body-negative groups) and we additionally showed between-stage comparisons for TDP-43 pathology.

To overcome some limitations of the neuropathological examination (e.g. only one hemisphere screened, a limited number of regions assessed, and a possible underestimation of the pathological burden) and provide a deeper understanding of the relationship between volume and TDP-43, we assessed the frequency of regional grey matter atrophy in all TDP-43-positive cases, irrespective of their TDP-43 stage. To do so, we first computed volumes adjusted for pathological (except TDP-43) and nuisance variables for a total of 43 MCALT regions of interest (41 non-cerebellar cortical regions of interest, and the hippocampus and amygdala) and for each TDP-43-positive case (i.e. *W*-scores) (Jack *et al.*, 1997). Specifically, we performed robust regressions in the TDP-43-negative group to estimate the effect of Braak and Lewy body stages, neuritic and diffuse amyloid- $\beta$  plaques, argyrophilic grain disease, vascular pathology, the time delay between MRI and death, age at MRI, sex, total intracranial volume and MRI field strength on volume. We then used the coefficients and residuals of these regressions to compute *W*-scores for each TDP-43-positive case using the following formula:

$$\text{W-score} = \frac{[(\text{patient's raw value}) - (\text{patient's expected value})]}{\text{standard deviation of the residuals in the TDP-43-negative group}} \quad (1)$$

where patient's expected value corresponded to the predicted value in the TDP-43-negative group given cases' Braak stage, Lewy body stage, age at MRI, etc. Using this procedure, we obtained a *W*-score for each region of interest and each TDP-43-positive case that represents how much the volume differs from the TDP-43-negative group taking into account the pathological and demographic variables of the subject. Similarly to *Z*-scores, *W*-scores have a mean value of 0 and a standard deviation (SD) of 1 in the reference group (i.e. TDP-43-negative group), and values of  $-1.65$  correspond to the 5th percentiles. Note that as robust regressions assign different weights to each subject to limit the weight of outliers

and better estimate regression coefficients, the mean of the *W*-scores was slightly different from 0 (range:  $-0.04$  to  $0.05$ ) but would be theoretically 0 if data did not contain any outliers.

*W*-scores were then used to define the brain regions most frequently atrophied in TDP-43-positive individuals when pathological features and covariates were regressed out. *W*-scores were binarized using a threshold of  $< -1.65$  (corresponding to a regional volume lower than 95th percentiles of the TDP-43-negative group) to examine the brain regions showing the highest percentage of TDP-43-positive cases with significant atrophy compared to the TDP-43-negative group. To assess if a brain region was more likely to present with atrophy than another, we performed conditional probability analyses. The theoretical background and details of this method for determining the sequential order of two conditions have been described in a previous article (Josephs *et al.*, 2016). In brief, we used McNemar's test to assess the evidence against the null hypothesis that the probability that (Region X presents with atrophy but not Region Y) is equally likely than (Region Y presents with atrophy but not Region X). This testing was performed for all combinations of regions of interest to generate a probabilistic sequential ordering for all 43 regions of interest. We used an uncorrected ( $P < 0.01$ ) threshold to determine whether we had sufficient evidence to reject the null hypothesis that two regions of interest were equally likely to be atrophied in the TDP-43-positive group.

Finally, we also assessed voxel-wise which brain regions were most likely to be atrophied in the TDP-43-positive group when accounting for pathological and demographic variables. To do so, we used the same procedure to compute voxel-wise *W*-scores (La Joie *et al.*, 2012). The *W*-score maps of the TDP-43-positive group were binarized using a threshold of  $< -1.65$  and used to compute a frequency map of grey matter atrophy (Ossenkoppele *et al.*, 2015; Perry *et al.*, 2017).

## Data availability

Mayo Clinic ADRC, ADPR and MCSA data used in this study are not currently publicly available for download.

## Results

### Population

A total of 407 individuals had complete pathological data and an antemortem MRI that passed visual quality control. Demographic data for the TDP-43-negative ( $n = 252$ ) and -positive ( $n = 155$ ) cases are presented in Table 1. Note that we added more than 200 new cases compared to previous studies from our laboratory assessing the relationship between TDP-43 and structural MRI [ $n = 93$  TDP-43-positive subjects overlap with Josephs *et al.* (2014a), and  $n = 103$  TDP-43-negative and 102 TDP-43-positive subjects overlap with Josephs *et al.* (2017a)].

Individuals with TDP-43 inclusions were older at the age of MRI and death than TDP-43-negative cases (Table 1). In agreement with previous studies, they were more likely to carry the *APOE*  $\epsilon 4$  allele (Josephs *et al.*, 2017a; Wennberg *et al.*, 2018;

**Table 1 Demographic and pathological data by TDP-43 status**

	TDP-43-negative (n = 252)	TDP-43-positive (n = 155)	P-value
Gender, female/male	105/147	87/68	0.006
Education, years	14.5 ± 3.1 <sup>a</sup>	14.6 ± 3.1	0.698
Age at MRI, years	78.4 ± 10.6	82.7 ± 7.8	<0.001
Age at death, years	81.8 ± 10.8	86.5 ± 8.2	<0.001
Time MRI to death, years	3.4 ± 2.3	3.8 ± 2.5	0.194
Clinical status, CUI/CI	85/167	25/130	<0.001
APOE ε4 carrier	101 (40.2%) <sup>a</sup>	89 (57.4%)	0.001
Braak stage			<0.001
0–II	58 (23.0%)	13 (8.4%)	
III	33 (13.1%)	10 (6.5%)	
IV	43 (17.1%)	15 (9.7%)	
V	36 (14.3%)	50 (32.3%)	
VI	82 (32.5%)	67 (43.2%)	
Neuritic amyloid-β plaques			0.004
0	45 (17.9%)	21 (13.5%)	
1	47 (18.7%)	11 (7.1%)	
2	53 (21.0%)	40 (25.8%)	
3	107 (42.5%)	83 (53.5%)	
Diffuse amyloid-β plaques			0.145
0	18 (7.1%)	10 (6.5%)	
1	17 (6.7%)	9 (5.8%)	
2	42 (16.7%)	14 (9.0%)	
3	175 (69.4%)	122 (78.7%)	
Lewy body stage			0.305
0	165 (65.5%)	88 (56.8%)	
1	12 (4.8%)	5 (3.2%)	
2	24 (9.5%)	21 (13.5%)	
3	36 (14.3%)	30 (19.4%)	
4	15 (6.0%)	11 (7.1%)	
Argyrophilic grain disease			0.264
0	215 (85.3%)	139 (89.7%)	
1	37 (14.7%)	16 (10.3%)	
Vascular pathology			0.252
0	144 (57.1%)	81 (52.3%)	
1	85 (33.7%)	64 (41.3%)	
2	23 (9.1%)	10 (6.5%)	

Unless otherwise indicated, values are mean ± SD. P-values refer to analyses of chi-squared and two-sample t-tests for categorical and continuous variables, respectively. Note that similar results were obtained when neuritic and diffuse amyloid-β plaques, and vascular pathology were treated continuously (as in the robust regressions). Refer to the 'Materials and methods' section for further details about the pathological stages. CI = cognitively impaired; CUI = cognitively unimpaired.

<sup>a</sup>Missing data for one participant.

Yang *et al.*, 2018) and be cognitively impaired at the time of MRI (Josephs *et al.*, 2015; James *et al.*, 2016). Comparisons of pathological variables revealed that TDP-43-positive cases had higher Braak stages and more neuritic amyloid-β plaques than TDP-43-negative cases. No significant difference was observed for diffuse amyloid-β plaques, Lewy body stage, argyrophilic grain disease and vascular pathology. Among the 155 TDP-43-positive individuals, 34 (21.9%) were at TDP-43 stage 1, 32 (20.6%) at stage 2, 14 (9%) at stage 3, and 75 (48%) at stage 4+ (32 at stage 4, 26 at stage 5 and 17 at stage 6). Demographic and pathological data by TDP-43 stages are presented in Supplementary Table 1, and details regarding regional TDP-43 distribution for each subject are provided in Supplementary Fig. 1.

## Region of interest analyses

Robust regressions explaining grey matter volume by pathological and demographic variables were performed in the brain regions targeted by TDP-43 pathology. These models fit the data well, as r-squared values ranged between 0.36 and 0.58 (mean: 0.51 ± 0.07) and adjusted r-squared values between 0.32 and 0.56 (mean: 0.48 ± 0.07) (Supplementary Table 2). Compared to the TDP-43-negative group, TDP-43 stage 1 was associated with bilateral loss of grey matter volume in the amygdala and entorhinal cortex (see Fig. 1 and Table 2 for estimates and P-values). Both TDP-43 stages 2 and 3 showed decreased grey matter volume in the entorhinal cortex and hippocampus. Individuals at TDP-43 stage 4+ presented with bilateral volume loss in the amygdala,

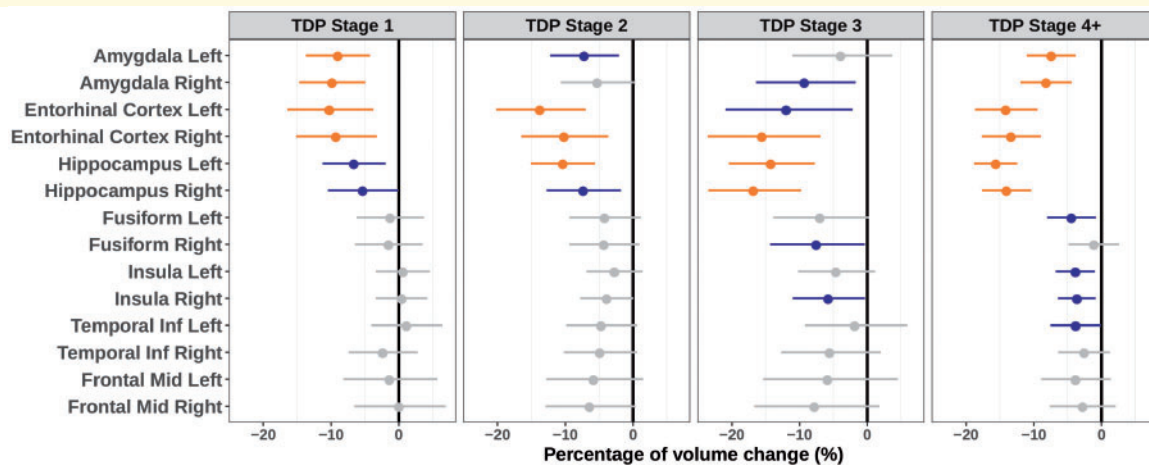


**Figure 1** Results of robust regressions showing the effect of TDP-43 stages on grey matter volume. Values represent the percentage of volume change, with 95% confidence intervals, associated with TDP-43 stages compared to the TDP-43-negative group. Colours indicate results that survived Bonferroni correction for multiple comparisons (orange,  $\alpha = 0.05$ ,  $P < 0.004$ , 14 models considered) or an uncorrected threshold of  $P < 0.05$  (blue). Columns indicate the pathological staging, and rows show the brain regions (i.e. dependent variables) ordered according to their progressive involvement with TDP-43 pathology.

entorhinal cortex, and hippocampus compared to TDP-43-negative cases. We also observed trends for volume loss in the fusiform and insula at TDP-43 stages 3 and 4+, although these findings did not survive Bonferroni correction. As shown in Fig. 1 and Table 2, the percentage of volume loss tended to increase in the entorhinal cortex and hippocampus with higher TDP-43 staging (i.e. ranging from  $-10.3\%$  to  $-5.4\%$  at stage 1 versus  $-15.7\%$  to  $-13.4\%$  at stage 4+). Estimates from the comparisons between the different TDP-43 stages further supported this effect (Supplementary Table 3). Yet, only the difference in hippocampal volume between TDP-43 stages 1 and 4+ survived the corrected statistical threshold [left hippocampus:  $-9.6\%$  ( $-14.5$ ,  $-4.5$ ),  $P < 0.001$ ; right hippocampus:  $-9.2\%$  ( $-14.6$ ,  $-3.4$ ),  $P = 0.002$ ].

The effects of Braak and Lewy body stages are presented in Table 2. In brief, Braak stage IV was associated with decreased volume in the amygdala, entorhinal cortex, and hippocampus compared to Braak stage 0–II. Braak stage V further involved the fusiform gyrus and insula, and Braak stage VI additionally involved the inferior temporal gyrus. Compared to individuals with no Lewy body pathology, cases with neocortical Lewy bodies (stage 3) showed decreased volume in the amygdala and entorhinal cortex. Finally, the presence of argyrophilic grain disease was associated with decreased volume in the amygdala (Supplementary Table 4). The effects on volume of Braak stage III, Lewy body stage 1, 2 and 4, diffuse and neuritic amyloid- $\beta$  plaques, and vascular pathology did not reach the statistical threshold (Table 2 and Supplementary Table 4).

Given that TDP-43-positive and -negative cases differed by Braak stage and neuritic plaque stage (Table 1), robust

regressions were repeated using a subsample of TDP-43-negative cases matched for pathological and demographic variables with the TDP-43-positive group. Specifically, we used the R package e1071 (Meyer *et al.*, 2018) to find TDP-43-negative individuals that matched as accurately as possible to TDP-43-positive cases for Braak and Lewy body stages, diffuse and neuritic amyloid- $\beta$  plaques, argyrophilic grain disease, vascular pathology, age at MRI, delay between MRI and death, sex and MRI field strength. The final matched subsample of TDP-43-negative cases ( $n = 155/252$ ) remained younger at the time of MRI ( $P < 0.001$ ) and death ( $P < 0.001$ ) than the TDP-43-positive group, but did not differ significantly for any other variables. Robust regressions in this subgroup ( $n = 310$ ) showed very similar results to those identified in the entire cohort (Supplementary Fig. 2).

## Voxel-wise analyses

Similar robust regressions assessing grey matter volume by pathological and demographic variables were performed voxel-wise. No significant differences were found at an FDR-corrected  $P < 0.001$  threshold between the TDP-43-negative group and either TDP-43 stage 1 or stage 2. When the statistical threshold was lowered ( $P < 0.001$  uncorrected,  $k > 500 \text{ mm}^3$ ), TDP-43 stage 1 showed bilateral volume loss in the amygdala and anterior hippocampus, and in the right more than left entorhinal cortex and ventral temporal pole (Fig. 2). TDP-43 stage 2 showed volume loss in the left amygdala, entorhinal cortex, anterior and posterior hippocampus, and ventral temporal pole. Compared to the TDP-43-negative group, TDP-43 stage 3 showed volume loss in

Table 2 Effect of TDP-43, tau and Lewy body stages on grey matter volume

	TDP stage I	TDP stage 2	TDP stage 3	TDP stage 4+
Amygdala L	-9.1 [-13.7, -4.2], P < 0.001	-7.3 [-12.2, -2.1], P = 0.007	-4 [-11.1, 3.7], P = 0.30	-7.5 [-11.1, -3.8], P < 0.001
Amygdala R	-9.9 [-14.7, -4.9], P < 0.001	-5.4 [-10.7, 0.3], P = 0.06	-9.4 [-16.4, -1.7], P = 0.02	-8.3 [-12, -4.4], P < 0.001
Entorhinal cortex L	-10.3 [-16.5, -3.7], P = 0.003	-13.8 [-20.2, -7], P < 0.001	-12 [-20.9, -2.2], P = 0.02	-14.2 [-18.7, -9.4], P < 0.001
Entorhinal cortex R	-9.4 [-15.2, -3.2], P = 0.003	-10.3 [-16.5, -3.6], P = 0.003	-15.6 [-23.6, -6.9], P < 0.001	-13.4 [-17.7, -9], P < 0.001
Hippocampus L	-6.7 [-11.2, -2], P = 0.006	-10.5 [-15.1, -5.6], P < 0.001	-14.3 [-20.4, -7.8], P < 0.001	-15.7 [-18.8, -12.4], P < 0.001
Hippocampus R	-5.4 [-10.5, 0], P = 0.05	-7.4 [-12.7, -1.8], P = 0.01	-16.9 [-23.5, -9.8], P < 0.001	-14.1 [-17.7, -10.4], P < 0.001
Fusiform L	-1.4 [-6.2, 3.7], P = 0.59	-4.3 [-9.4, 1.2], P = 0.12	-7.1 [-13.9, 0.3], P = 0.06	-4.5 [-8, -0.8], P = 0.02
Fusiform R	-1.6 [-6.5, 3.5], P = 0.53	-4.4 [-9.4, 1], P = 0.11	-7.6 [-14.3, -0.4], P = 0.04	-1.2 [-4.9, 2.6], P = 0.53
Insula L	0.5 [-3.4, 4.6], P = 0.79	-2.8 [-6.9, 1.4], P = 0.19	-4.7 [-10.2, 1.2], P = 0.12	-3.9 [-6.8, -1], P = 0.010
Insula R	0.4 [-3.4, 4.2], P = 0.85	-4 [-7.8, 0], P = 0.05	-5.8 [-11, -0.3], P = 0.04	-3.7 [-6.4, -0.9], P = 0.01
Temporal inferior L	1.1 [-4, 6.4], P = 0.69	-4.8 [-9.9, 0.6], P = 0.08	-1.9 [-9.2, 5.9], P = 0.62	-3.9 [-7.5, -0.1], P = 0.05
Temporal inferior R	-2.4 [-7.4, 2.8], P = 0.35	-5 [-10.2, 0.6], P = 0.08	-5.6 [-12.7, 2], P = 0.14	-2.7 [-6.4, 1.2], P = 0.18
Frontal middle L	-1.5 [-8.2, 5.7], P = 0.68	-5.9 [-12.8, 1.5], P = 0.12	-5.9 [-15.4, 4.5], P = 0.25	-3.9 [-8.9, 1.4], P = 0.14
Frontal middle R	-0.1 [-6.6, 6.9], P = 0.99	-6.5 [-12.9, 0.4], P = 0.06	-7.9 [-16.7, 1.8], P = 0.11	-2.9 [-7.6, 2.1], P = 0.25
	<b>Braak stage III</b>	<b>Braak stage IV</b>	<b>Braak stage V</b>	<b>Braak stage VI</b>
Amygdala L	-1.9 [-7, 3.4], P = 0.47	-8.7 [-13.4, -3.7], P < 0.001	-9.9 [-15.1, -4.4], P < 0.001	-15.1 [-20.2, -9.8], P < 0.001
Amygdala R	-1.6 [-7, 4], P = 0.56	-7.6 [-12.7, -2.3], P = 0.006	-11 [-16.5, -5.3], P < 0.001	-12.3 [-17.8, -6.4], P < 0.001
Entorhinal cortex L	-1.7 [-8.7, 5.7], P = 0.64	-10.9 [-17.2, -4.1], P = 0.002	-12.5 [-19.4, -4.9], P = 0.002	-18.2 [-24.8, -10.9], P < 0.001
Entorhinal cortex R	0.1 [-6.5, 7.2], P = 0.97	-7.4 [-13.5, -0.8], P = 0.03	-7.3 [-14.1, 0.2], P = 0.06	-13.7 [-20.3, -6.7], P < 0.001
Hippocampus L	-2.1 [-7, 3.1], P = 0.42	-12.2 [-16.6, -7.6], P < 0.001	-11.3 [-16.3, -6], P < 0.001	-17.6 [-22.4, -12.5], P < 0.001
Hippocampus R	-0.7 [-6.2, 5.2], P = 0.81	-9.2 [-14.2, -3.9], P < 0.001	-10.8 [-16.4, -4.9], P < 0.001	-15 [-20.4, -9.2], P < 0.001
Fusiform L	0.1 [-5, 5.5], P = 0.97	-2.5 [-7.5, 2.7], P = 0.34	-4.2 [-9.7, 1.6], P = 0.15	-15.1 [-20.1, -9.9], P < 0.001
Fusiform R	0.1 [-5, 5.5], P = 0.98	-2.2 [-7.2, 3], P = 0.39	-8.2 [-13.4, -2.6], P = 0.004	-16.1 [-21, -10.9], P < 0.001
Insula L	-1 [-5, 3.2], P = 0.65	-3.8 [-7.7, 0.3], P = 0.07	-6.9 [-11.2, -2.5], P = 0.003	-12.7 [-16.7, -8.4], P < 0.001
Insula R	-1.8 [-5.6, 2.2], P = 0.36	-4.3 [-8, -0.4], P = 0.03	-7.6 [-11.7, -3.3], P < 0.001	-10.7 [-14.7, -6.5], P < 0.001
Temporal inferior L	0.1 [-5, 5.5], P = 0.97	-2.2 [-7.3, 3.2], P = 0.41	-4.9 [-10.4, 0.9], P = 0.10	-16.7 [-21.7, -11.5], P < 0.001
Temporal inferior R	0.8 [-4.5, 6.4], P = 0.77	-1.2 [-6.4, 4.3], P = 0.65	-7.7 [-13.2, -1.9], P = 0.010	-16.2 [-21.3, -10.8], P < 0.001
Frontal middle L	-5.2 [-11.9, 2], P = 0.15	-2.9 [-9.8, 4.5], P = 0.43	-3 [-10.7, 5.4], P = 0.47	-9.7 [-17, -1.6], P = 0.02
Frontal middle R	-5.6 [-12, 1.3], P = 0.11	-1.2 [-7.8, 5.9], P = 0.73	-2 [-9.3, 6], P = 0.62	-7.1 [-14.2, 0.7], P = 0.07
	<b>Lewy body stage I</b>	<b>Lewy body stage 2</b>	<b>Lewy body stage 3</b>	<b>Lewy body stage 4</b>
Amygdala L	1.2 [-5.4, 8.2], P = 0.73	-5.1 [-9.3, -0.7], P = 0.02	-7.5 [-11.1, -3.6], P < 0.001	-1.2 [-6.6, 4.7], P = 0.69
Amygdala R	-0.7 [-7.6, 6.7], P = 0.84	-5.6 [-10, -1], P = 0.02	-4.5 [-8.5, -0.3], P = 0.03	1.2 [-4.8, 7.6], P = 0.70
Entorhinal cortex L	-2.5 [-11.2, 7.2], P = 0.60	-5.3 [-11, 0.7], P = 0.08	-7.9 [-12.9, -2.7], P = 0.004	-2.4 [-9.9, 5.7], P = 0.54
Entorhinal cortex R	-0.1 [-8.4, 8.9], P = 0.98	-4.2 [-9.6, 1.5], P = 0.15	-3 [-7.9, 2.2], P = 0.25	1.8 [-5.5, 9.8], P = 0.63
Hippocampus L	0 [-6.3, 6.7], P = 0.99	-4.9 [-9, -0.6], P = 0.03	-2.7 [-6.5, 1.1], P = 0.16	0.8 [-4.7, 6.6], P = 0.78
Hippocampus R	-3.2 [-10, 4.1], P = 0.38	-6.4 [-10.9, -1.7], P = 0.008	-1 [-5.2, 3.4], P = 0.65	3.5 [-2.9, 10.2], P = 0.29
Fusiform L	-1.6 [-7.9, 5.2], P = 0.64	-5.5 [-9.6, -1.2], P = 0.01	-1.6 [-5.4, 2.4], P = 0.43	5.3 [-0.7, 11.6], P = 0.08
Fusiform R	-1.1 [-7.4, 5.6], P = 0.74	-2.8 [-6.9, 1.6], P = 0.21	-1 [-4.8, 3], P = 0.62	2.2 [-3.5, 8.4], P = 0.45
Insula L	-1.4 [-6.5, 3.9], P = 0.59	-1.1 [-4.5, 2.4], P = 0.53	-0.4 [-3.5, 2.8], P = 0.81	-0.7 [-5.1, 3.9], P = 0.77
Insula R	-2 [-6.8, 3], P = 0.42	1.4 [-4.6, 2], P = 0.42	0 [-3.9, 4], P = 1.00	-1.2 [-5.4, 3.2], P = 0.59
Temporal inferior L	1.3 [-5.4, 8.4], P = 0.72	-3.6 [-7.8, 0.8], P = 0.11	0.3 [-3.7, 4.5], P = 0.87	-3.4 [-8.9, 2.5], P = 0.25
Temporal inferior R	0.3 [-6.4, 7.5], P = 0.93	-3.9 [-8.2, 0.5], P = 0.08	5.4 [-0.3, 11.5], P = 0.06	0 [-5.7, 6.1], P = 0.99
Frontal middle L	1.8 [-7.4, 12], P = 0.71	1.4 [-4.7, 7.9], P = 0.66	0.9 [-4.3, 6.3], P = 0.75	2.4 [-5.5, 11.1], P = 0.56
Frontal middle R	-5 [-13.1, 4], P = 0.27	-3 [-8.6, 2.8], P = 0.30		1.8 [-5.6, 9.8], P = 0.64

Results of the robust regressions showing the effect of TDP-43, tau (Braak) and Lewy body stages on grey matter volume. Values represent the percentage of volume change [95% confidence intervals] associated with TDP-43, Braak, and Lewy Body stages compared to TDP-43-negative, Braak Stage 0-I, and Lewy body-negative groups, respectively. Results in bold survived Bonferroni correction for multiple comparisons ( $\alpha = 0.05$ ,  $P < 0.004$ , 14 models considered). L = left; R = right.

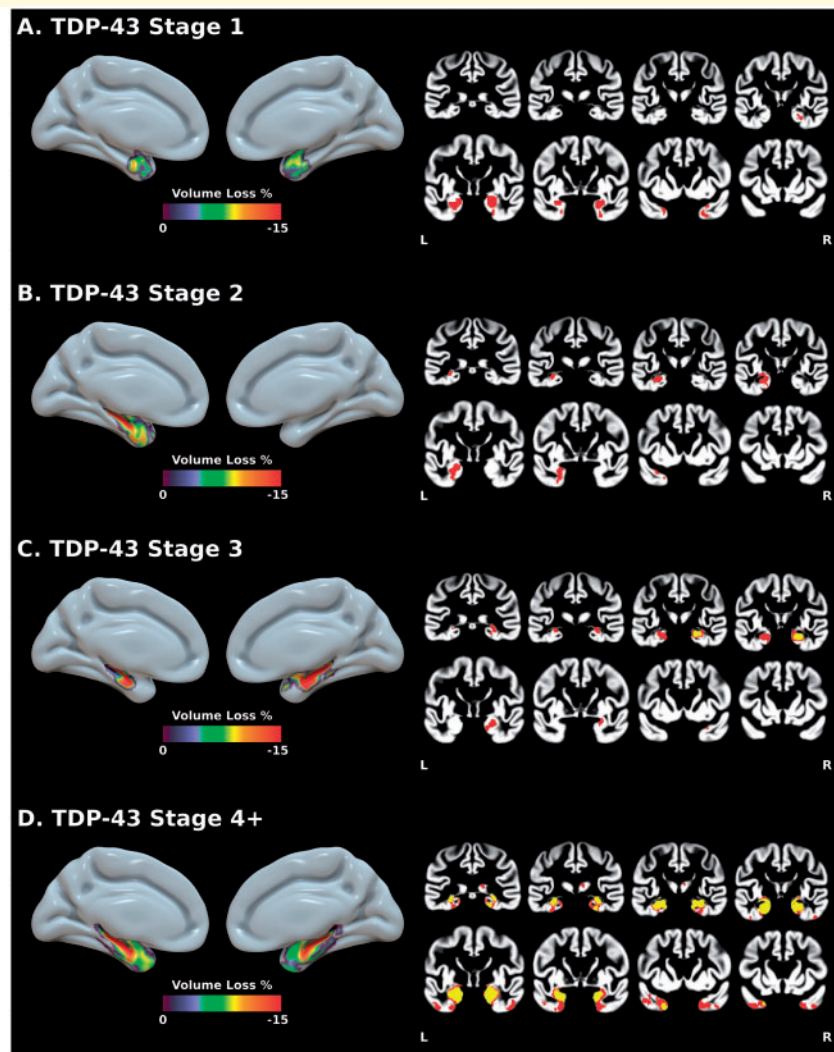


**Figure 2** Results of voxel-wise robust regressions showing the effect of TDP-43 stages on grey matter volume. Values represent the percentage of volume change associated with TDP-43 stages compared to the TDP-43-negative group. Coronal slices show both  $P < 0.001$  FDR-corrected (yellow) and  $P < 0.001$  uncorrected (red) results ( $k > 500 \text{ mm}^3$ ). Results are presented in neurological convention. L = left; R = right.

the right anterior hippocampus that extended, at an uncorrected threshold ( $P < 0.001$ ), into the right posterior hippocampus, amygdala, entorhinal cortex, ventral pole, and parahippocampal gyrus, and into the left hippocampus, amygdala and entorhinal cortex. Finally, the TDP-43 stage 4+ group was characterized by the bilateral involvement of the whole hippocampus and amygdala, the entorhinal cortex, ventral temporal pole, and right parahippocampal gyrus. At an uncorrected threshold, this pattern extended into the temporal pole and further encompassed the fusiform gyrus, left parahippocampal gyrus and right thalamus.

Between TDP-43 stage comparisons did not reveal significant differences at the FDR-corrected  $P < 0.001$  threshold. At an uncorrected threshold ( $P < 0.001$ ), comparisons with TDP-43 stage 1 showed volume loss in the right hippocampus at TDP-43 stage 3, and in the bilateral

hippocampus and right thalamus at TDP-43 stage 4+ (Supplementary Fig. 3). Finally, the relationships between grey matter volumes and Braak and Lewy body stages, and argyrophilic grain disease are presented in Supplementary Figs 4 and 5. Briefly, volume loss was mainly found in medial temporal structures at Braak stage IV, additionally included the posterior cingulate at Braak stage V and most temporo-parietal, lateral occipital and frontal regions at Braak stage VI. Lewy body stage 2 (limbic stage) was associated with decreased volume in the left parietal cortex, and stage 3 (neocortical stage) with volume loss in the left amygdala and anterior hippocampus. The presence of argyrophilic grain disease was associated with decreased volume in the left amygdala and anterior hippocampus. No associations were obtained with diffuse and neuritic amyloid- $\beta$  plaques, and with vascular pathology.



## Regions most frequently atrophied with TDP-43

Grey matter volumes were converted, for each region of interest and each TDP-43-positive case, into *W*-scores adjusted for pathological (i.e. Braak and Lewy body stages, diffuse and neuritic amyloid- $\beta$  plaques, argyrophilic grain disease and vascular pathology) and nuisance variables. We then used a threshold of *W*-score  $< -1.65$  to determine the presence of significant atrophy compared to the TDP-43-negative group. Note that a *W*-score  $< -1.65$  corresponds to a volume below the 95th percentile of the TDP-43-negative cases after taking into account the pathological scores and demographic features of the subject.

Results showed that the hippocampus was the most frequently atrophied brain region of interest in TDP-43-positive cases (32.9%, Fig. 3). It was followed by the amygdala (24.5%), entorhinal cortex (22.6%), middle (20%) and superior (13.5%) temporal poles, inferior temporal gyrus (12.9%), fusiform (12.9%) and parahippocampal (11.6%) gyri. When we used a dynamic range to define the presence of atrophy (*W*-scores  $< -0.5$  to *W*-scores  $< -2$ ), we consistently observed that (i) the hippocampus was the most atrophied brain region; (ii) followed by either the amygdala or the entorhinal cortex; and then (iii) the middle temporal pole (Fig. 3). The order between the other regions of interest was more threshold-dependent but the superior temporal pole, inferior temporal, fusiform and parahippocampal gyri tended to be systematically more atrophied than any other regions of interest.

## Conditional probability analyses

The *W*-scores were then used to compute pairwise conditional probability to further understand the sequential grey

matter atrophy associated with TDP-43 pathology. Specifically, this analysis used individual profiles to determine the likelihood of one brain region to be atrophied before another. Results showed that the hippocampus had a significantly higher probability to show grey matter loss before any other regions except the amygdala (Fig. 4). The amygdala, entorhinal cortex, and middle temporal pole did not differ in their probability to be atrophied first but were significantly more likely to be atrophied before most other brain regions (except the superior temporal pole, the fusiform and inferior temporal gyri for the entorhinal cortex and middle temporal pole). Finally, a third cluster of regions of interest, including the superior temporal pole, fusiform, inferior temporal and parahippocampus gyri, appear more likely to show grey matter loss than several other brain regions.

## Frequency map

*W*-scores adjusted for pathological scores and covariates were also computed voxel-wise for each TDP-43-positive case and used to create a frequency map of grey matter atrophy (using, as previously, a threshold of *W*-score  $< -1.65$  to determine significant atrophy compared to the TDP-43-negative group). Results showed that the hippocampus (especially its anterior portion) and the amygdala were the regions that most frequently showed atrophy ( $>30\%$ ) in the TDP-43-positive group (Fig. 5). These regions were followed by the ventral temporal pole and entorhinal cortex (25–30%), and then by the dorsal temporal pole, parahippocampus, anterior inferior temporal and fusiform gyri (15–25%). Finally, the posterior insula (at the junction of the superior temporal gyrus),

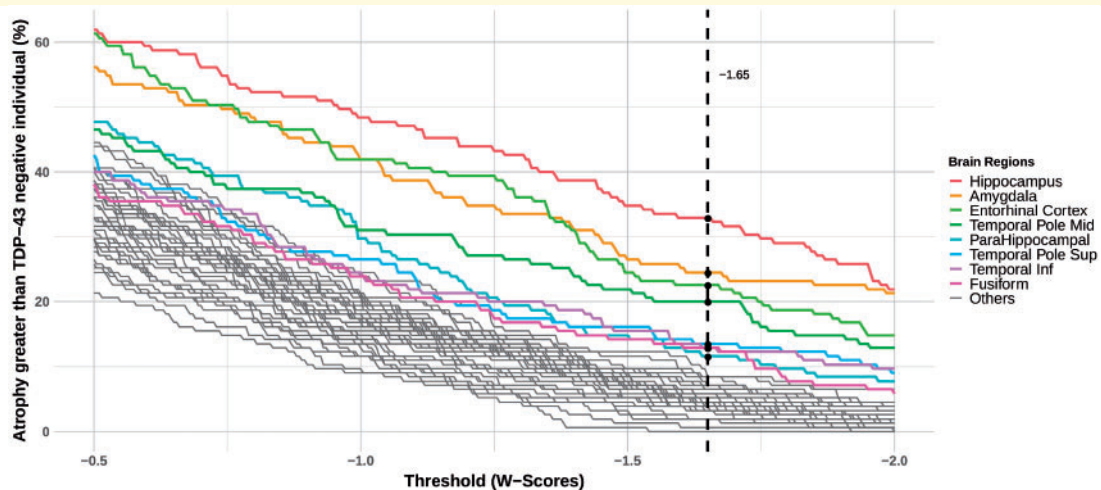


**Figure 3** Effect of *W*-score threshold on the percentage of TDP-43-positive cases showing more grey matter atrophy than TDP-43-negative cases. *W*-scores were computed using the TDP-43-negative cases ( $n = 252$ ) as the reference group, and represent grey matter volume adjusted for Braak stage, Lewy body stage, diffuse and neuritic amyloid- $\beta$  plaques, argyrophilic grain disease, vascular pathology, and covariates. Colours were used for the regions showing most frequently grey matter atrophy in the TDP-43-positive versus TDP-43-negative cases. Brain regions on the right are ordered by the area under the curve.

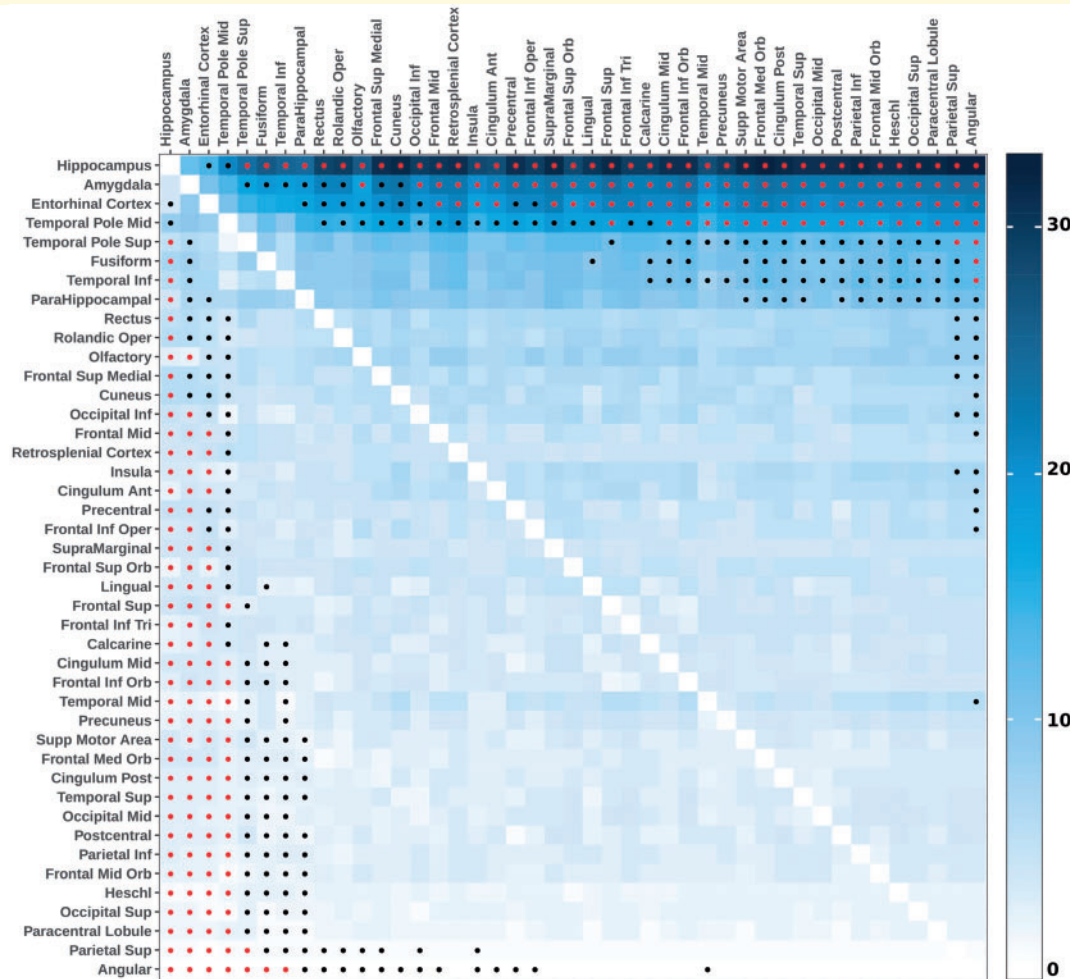


**Figure 4** Pairwise conditional probability matrix showing the probability of grey matter volume loss in each brain region compared to other brain regions in TDP-43-positive cases. Reading the plot from left to right, the conditional probability estimates (%) show the estimated probability that the region on the left shows grey matter volume loss before the region on the right. Reading from top to bottom, the entries show the estimated probability that the region below shows grey matter volume loss before the region above. Dots indicate results that were statistically significant at the  $P < 0.01$  level (black) and that survived Bonferroni correction for multiple comparisons (red,  $\alpha = 0.05$ ,  $P < 0.00006$ , 903 models considered).  $P$ -values were assessed using exact McNemar's test, and a region was considered having grey matter volume loss when  $W$ -score  $< -1.65$  (i.e. volume below the 95th percentiles of the TDP-43-negative group after accounting for pathological scores and covariates).

orbitofrontal cortex and gyrus rectus were involved in ~15% of the cases.

## Discussion

In the present study, we aimed at better characterizing the pattern of grey matter loss associated with the pattern of TDP-43 spread independently of other age-related neuropathologies in a heterogeneous cohort of non-FTLD cases. We found that the extent of TDP-43 pathology is related to the extent of grey matter atrophy. Specifically, our results showed a gradual loss of volume in medial temporal lobe regions associated with increasing TDP-43 stage. We also observed the progressive involvement of lateral temporal, insular and frontal regions with TDP-43 advancement.

Additional analyses revealed a sequential pattern of grey matter atrophy related to TDP-43 pathology that starts in medial temporal structures, with early involvement of the temporal pole and then extension into other neocortical regions. Together, these results demonstrate the unique contribution of TDP-43 pathology on brain structure and shed light on the regional distribution of TDP-43-related atrophy, and possibly TDP-43 pathology itself, in non-FTLD individuals.

Our findings demonstrated an early and independent effect of TDP-43 pathology on grey matter volume of the amygdala. Indeed, we found that individuals with TDP-43 inclusions limited to the amygdala (stage 1) presented with less volume in this region than subjects without TDP-43 after controlling for tau, amyloid- $\beta$ , Lewy body, argyrophilic grain disease, and vascular pathologies. This result

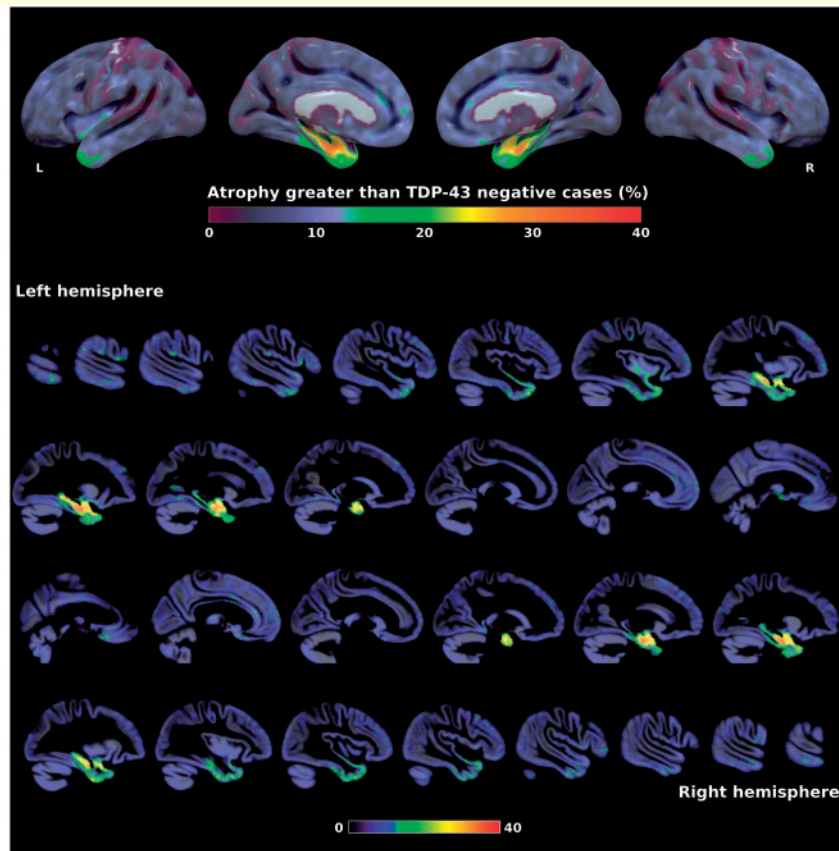


**Figure 5** Frequency map of grey matter atrophy in TDP-43-positive cases compared to TDP-43-negative cases. Values represent the percentage of TDP-43-positive cases having significantly more atrophy than the TDP-43-negative group ( $W$ -score  $< -1.65$ ) accounting for Braak stage, Lewy body stage, diffuse and neuritic amyloid- $\beta$  plaques, argyrophilic grain disease, vascular pathology, age at MRI, time MRI to death, sex, total intracranial volume, and MRI magnetic field. Results are presented in neurological convention. L = left; R = right.

remained significant when TDP-43-positive cases were compared to a subsample of TDP-43-negative subjects matched for pathological variables (including Alzheimer's disease). To our knowledge, this is the first evidence of a neuroimaging correlate of TDP-43 pathology in the amygdala only. Indeed, our previous investigations in the Alzheimer's disease spectrum did not find an effect of TDP-43 stage 1 on grey matter volume (Josephs *et al.*, 2014a, 2017a). This discrepancy might be explained by the larger sample size, the difference in population and the use of additional pathological covariates in the present study.

Intriguingly, individuals at TDP-43 stage 1, with no TDP-43 beyond the amygdala, showed additional grey matter loss in the entorhinal cortex, anterior hippocampus and ventral portion of the temporal pole. Given that neurons in the amygdala have direct projections toward these regions (Marino *et al.*, 2016; Nelson *et al.*, 2018), and vice versa, it is possible that these losses of volume reflect a distant effect of the neurodegeneration in the amygdala. Histopathological changes in regions connected to an injured area have been described previously following focal cerebral infarction (Duering *et al.*, 2012; Zhang *et al.*, 2012), and similar cellular mechanisms (e.g. retrograde

degeneration, anterograde trans-synaptic degeneration) may lead to remote effects of the amygdala atrophy. Alternatively, the TDP-43 staging may have been underestimated for some individuals as only one hemisphere (the left most often) was assessed for the presence of TDP-43 inclusions. Finally, we cannot rule out that other pathological variables not assessed in the present study (e.g. arteriosclerosis) may have influenced the volume of these regions.

The spread of TDP-43 pathology (stage 2 to 4+) was associated with decreased volume of the amygdala, entorhinal cortex and hippocampus compared to the TDP-43-negative group. The effect of TDP-43 stage 2 and 3 on amygdala volume did not reach significance in the region of interest analyses when the threshold was corrected for multiple comparisons. However, the involvement of this structure was retrieved at a lower statistical threshold ( $P < 0.05$ ) and when analyses were performed voxel-wise. Even though comparisons between TDP-43 stages showed limited differences, possibly due to the lack of statistical power resulting from the relatively small sample size for each TDP-43 stage, our results suggest the progressive involvement of the entorhinal cortex and hippocampus with

TDP-43 advancement. Indeed, the percentage of volume loss in these regions tended to be higher, and confidence intervals smaller (apart for the smallest group, i.e. TDP-43 stage 3), with increasing TDP-43 stages (see also statistical trends for difference between TDP-43 stages in Supplementary Table 3). Moreover, voxel-wise results showed a clear progression of hippocampal atrophy along the anteroposterior axis with advancing TDP-43 stages: effects of TDP-43 pathology were first localized in the most anterior portion of the hippocampus and gradually involved more posterior regions. This is in agreement with previous evidence showing a stronger effect of TDP-43 on the anterior than the posterior hippocampus (Hanko *et al.*, 2018). Finally, when treated as a continuous variable, TDP-43 staging was associated with volume change in the amygdala, entorhinal cortex, and hippocampus (data not shown). Altogether, these results support a progressive effect of TDP-43 on medial temporal volumes. We hypothesize that TDP-43 pathology accumulates locally while spreading within these regions and that both phenomena contribute to the gradual volume loss associated with increasing TDP-43 stages. Future studies combining both extent and severity measurements could provide further insight into these pathological processes.

In a recent study on the entity limbic-predominant age-related TDP-43 encephalopathy (LATE), Nelson and colleagues (2019) suggested using a collapsed three stages scheme for routine pathological screening of TDP-43 but supported the use of the extended TDP-43 staging schemes (Josephs *et al.*, 2016; Nag *et al.*, 2018) for research. The progressive involvement of medial temporal structures with TDP-43 staging, together with previous evidence showing cognitive differences between collapsed stages (Josephs *et al.*, 2014a; Nag *et al.*, 2018), further emphasizes the importance of not collapsing the TDP-43 staging scheme into lesser number of stages for research (Josephs *et al.*, 2019a).

Another novel aspect of this study was the use of an approach that regressed out the effect of pathological variables (i.e. Braak neurofibrillary tangle and Lewy body stages, diffuse, and neuritic amyloid- $\beta$  plaque burden, argyrophilic grain disease, and vascular pathology) on grey matter volume in order to examine the sequential grey matter loss related to TDP-43. These analyses confirmed the particular vulnerability of medial temporal structures to TDP-43 pathology, with the amygdala, entorhinal cortex and hippocampus being the most frequently atrophied regions of interest. Even though the conditional probability analyses did not reveal any significant difference between the hippocampus and the amygdala in their probability to be atrophied one before another, the hippocampus was the most frequently atrophied brain region in TDP-43-positive cases and the effect of TDP-43 staging appears to be more gradual in this region than in the amygdala. This result may reflect the distinct vulnerability of these structures to TDP-43-related toxicity, i.e. the subpopulations of neurons most prone to shrink or death in response to the presence of any TDP-43 pathology might be

more prevalent in the hippocampus than in the amygdala. The particular vulnerability of the hippocampal region is further supported by the well-established co-existence of hippocampal sclerosis with TDP-43 pathology (Amador-Ortiz *et al.*, 2007; Nelson *et al.*, 2016). Alternatively, inclusions of TDP-43 in the amygdala may be confined to some subnuclei which, in turn, limit the sensitivity to detect progressive grey matter atrophy with standard structural MRI.

Beyond these structures, previously identified as altered by the presence of TDP-43 pathology (Josephs *et al.*, 2008a, 2014a, b, 2015, 2017a; Kovacs *et al.*, 2013; Hanko *et al.*, 2018; Makkinejad *et al.*, 2019), our results highlighted the early involvement of the middle temporal pole. Indeed, this region was the fourth region of interest most frequently atrophied in the TDP-43-positive group and was more likely to demonstrate volume loss before most other regions of interest. The voxel-wise frequency map further showed that it is especially the ventral portion, adjacent to the amygdala, that is most frequently damaged in TDP-43-positive subjects. According to Nag *et al.* (2018), TDP-43 affects the temporal pole early in the progression of TDP-43 pathology, shortly after the involvement of medial temporal structures and before other neocortical areas. Given that the temporal pole is highly interconnected to the amygdala (Olson *et al.*, 2007; Marino *et al.*, 2016), it is plausible that TDP-43 pathology develops early in this region while spreading in parallel into other medial temporal structures. This may explain why each TDP-43 stage was associated with volume loss in this region in the voxel-wise regressions.

Our results also revealed the deleterious effect of TDP-43 in other temporal and frontal regions. We found decreased volume in the parahippocampal gyrus at TDP-43 stage 3 and 4+, and in the fusiform gyrus and thalamus at stage 4+ only. The posterior insula, orbitofrontal cortex, and gyrus rectus also presented with relatively frequent grey matter loss ( $\pm 15\%$  of the TDP-43-positive cases) despite not being significantly associated with any TDP-43 stages. All these regions have been shown to be targeted by TDP-43 pathology in non-FTLD cases (Josephs *et al.*, 2014a, 2016; Nag *et al.*, 2018). TDP-43 inclusions were previously reported in the thalamus (Cykowski *et al.*, 2016), but this region has not yet been associated with a specific stage. Our results suggest it is involved relatively late.

To our knowledge, few studies assessed voxel-wise effects of distinct pathologies on grey matter volume (for a review on radiological-pathological findings, see Dallaire-Th eroux *et al.*, 2017). In agreement with those related to tau (Whitwell *et al.*, 2008, Josephs *et al.*, 2014b; Kotrotsou *et al.*, 2015), we found a progressive involvement of medial temporal structures at Braak stage IV, that extended into temporal and medial parietal regions at Braak stage V, and finally encompassed most temporo-parietal regions at Braak stage VI. Interestingly, this pattern partially overlaps with the one related to TDP-43 pathology. This is not surprising given that both pathologies target common

brain regions such as the amygdala, entorhinal cortex, hippocampus, or inferior temporal gyrus. Yet, the specificity of our results is supported by the lack of significant association between volume and TDP-43 in brain regions targeted by tau but not by TDP-43. Hence, only tau pathology was associated with volume loss in medial and lateral parietal cortex, and these regions did not show frequent atrophy in the TDP-43-positive group once the effect of pathological variables (including tau) was regressed out (Fig. 5). In line with previous studies (Josephs *et al.*, 2008b; Burton *et al.*, 2012), our results further showed decreased medial temporal lobe volume in the presence of argyrophilic grain disease and Lewy body pathology (at the neocortical stage but note also trends for effects at the limbic stage). By contrast, we did not find an effect of amyloid- $\beta$  and vascular pathologies on grey matter volume. Importantly, the percentage of volume loss associated with TDP-43 and tau were comparable, and the earliest TDP-43 stages appeared to have at least similar, and possibly more, influence on medial temporal volume than the earliest Braak stages. It is worth mentioning, however, that, unlike TDP-43, Braak stage estimates were not computed as compared to a tau-negative group as very few individuals ( $n = 2$ ) were at Braak stage 0. Additional studies are therefore needed to better compare the relative effects of each pathology on grey matter volume.

This study has some limitations. First, despite a large pathological cohort, the relatively small sample size for some TDP-43 stages ( $n = 14$  to 34 for stages 1–3) may have prevented us from detecting the effect of TDP-43 in some brain regions. Second, we used cross-sectional T<sub>1</sub>-structural images acquired on MRI scanners with different field strength and sometimes several years before death. Nonetheless, we controlled for these variables in all our analyses and results remained highly similar when groups were matched. Third, while we regressed out several pathological variables, we used some measurements of extent (e.g. Braak staging for tau pathology) or presence/absence (e.g. argyrophilic grain disease) that do not account for the burden of pathology. Future studies could, therefore, include more refined pathological scores to further disentangle the specific effect of each pathology on grey matter atrophy. Finally, we interpreted our results in a causal perspective where pathologies (e.g. TDP-43, tau) lead to neurodegeneration. Yet, the exact processes that relate these pathologies to neurodegeneration remain unclear and further investigations are required to support this causality.

In summary, this study demonstrated the detrimental and independent effect of TDP-43 on grey matter volume in non-FTLD brains. These effects likely explain the associations between TDP-43 and both decreased cognitive performances and increased likelihood of dementia (Josephs *et al.*, 2008a; Nag *et al.*, 2015; Boyle *et al.*, 2018). Together, these findings highlight that TDP-43 is a major cause of neurodegeneration in older adults and a crucial target for future disease-modifying drugs.

## Acknowledgements

Authors are grateful to K. Johnson for her help with the pathological data, and to Dr E. Arenaza-Urquijo for her scientific inputs and technical advices.

## Funding

This research was funded by the National Institutes of Health (grants R01 AG011378, R01 AG015866, R01 AG034676, R01 AG037491, R01 AG041851, R01 NS097495, P50 AG016574, U01 AG006786 and U01 NS100620), Gerald and Henrietta Rauenhorst Foundation, Elsie and Marvin Dekelboum Family Foundation, Alexander Family Alzheimer's Disease Research Professorship of the Mayo Clinic, Mayo Foundation for Medical Education and Research, the Fondation Thérèse et René Planiol and Conseil Régional de Normandie.

## Competing interests

Matthew L. Senjem owns or has owned shares of the following medical related stocks, unrelated to the current work, within past three years: Align Technology, Inc., CRISPR Therapeutics, Gilead Sciences, Inc., Globus Medical Inc., Inovio Biomedical Corp., Ionis Pharmaceuticals, Johnson & Johnson, LHC Group, Inc., Medtronic, Inc., Mesa Laboratories, Inc., Natus Medical Incorporated, Parexel International Corporation, Varex Imaging Corporation. None of the others investigators of this study have any conflicts of interest.

## Supplementary material

Supplementary material is available at *Brain* online.

## References

- Amador-Ortiz C, Lin W-L, Ahmed Z, Personett D, Davies P, Duara R, et al. TDP-43 immunoreactivity in hippocampal sclerosis and Alzheimer's disease. *Ann Neurol* 2007; 61: 435–45.
- Arai T, Hasegawa M, Akiyama H, Ikeda K, Nonaka T, Mori H, et al. TDP-43 is a component of ubiquitin-positive tau-negative inclusions in frontotemporal lobar degeneration and amyotrophic lateral sclerosis. *Biochem Biophys Res Commun* 2006; 351: 602–11.
- Arai T, Mackenzie IRA, Hasegawa M, Nonaka T, Niizato K, Tsuchiya K, et al. Phosphorylated TDP-43 in Alzheimer's disease and dementia with Lewy bodies. *Acta Neuropathol* 2009; 117: 125–36.
- Ashburner J, Friston KJ. Unified segmentation. *Neuroimage* 2005; 26: 839–51.
- Avants BB, Epstein CL, Grossman M, Gee JC. Symmetric diffeomorphic image registration with cross-correlation: evaluating automated labeling of elderly and neurodegenerative brain. *Med Image Anal* 2008; 12: 26–41.

- Boyle PA, Yu L, Wilson RS, Leurgans SE, Schneider JA, Bennett DA. Person-specific contribution of neuropathologies to cognitive loss in old age. *Ann Neurol* 2018; 83: 74–83.
- Braak H, Braak E. Neuropathological staging of Alzheimer-related changes. *Acta Neuropathol* 1991; 82: 239–59.
- Burton EJ, Mukaetova-Ladinska EB, Perry RH, Jaros E, Barber R, O'Brien JT. Neuropathological correlates of volumetric MRI in autopsy-confirmed Lewy body dementia. *Neurobiol Aging* 2012; 33: 1228–36.
- Cairns NJ, Bigio EH, Mackenzie IRA, Neumann M, Lee VM-Y, Hatanpaa KJ, et al. Neuropathologic diagnostic and nosologic criteria for frontotemporal lobar degeneration: consensus of the Consortium for Frontotemporal Lobar Degeneration. *Acta Neuropathol* 2007; 114: 5–22.
- Cykowski MD, Takei H, Van Eldik LJ, Schmitt FA, Jicha GA, Powell SZ, et al. Hippocampal sclerosis but not normal aging or Alzheimer disease is associated with TDP-43 pathology in the basal forebrain of aged persons. *J Neuropathol Exp Neurol* 2016; 75: 397–407.
- Dallaire-Thérout C, Callahan BL, Potvin O, Saikali S, Duchesne S. Radiological-pathological correlation in Alzheimer's disease: systematic review of antemortem magnetic resonance imaging findings. *J Alzheimers Dis* 2017; 57: 575–601.
- Duering M, Righart R, Csanadi E, Jouvent E, Hervé D, Chabriat H, et al. Incident subcortical infarcts induce focal thinning in connected cortical regions. *Neurology* 2012; 79: 2025–8.
- Fujishiro H, Uchikado H, Arai T, Hasegawa M, Akiyama H, Yokota O, et al. Accumulation of phosphorylated TDP-43 in brains of patients with argyrophilic grain disease. *Acta Neuropathol* 2009; 117: 151–8.
- Hanko V, Apple AC, Alpert KI, Warren KN, Schneider JA, Arfanakis K, et al. In vivo hippocampal subfield shape related to TDP-43, amyloid beta, and tau pathologies. *Neurobiol Aging* 2018; 74: 171–81.
- Higashi S, Iseki E, Yamamoto R, Minegishi M, Hino H, Fujisawa K, et al. Concurrence of TDP-43, tau and alpha-synuclein pathology in brains of Alzheimer's disease and dementia with Lewy bodies. *Brain Res* 2007; 1184: 284–94.
- Hu WT, Josephs KA, Knopman DS, Boeve BF, Dickson DW, Petersen RC, et al. Temporal lobar predominance of TDP-43 neuronal cytoplasmic inclusions in Alzheimer disease. *Acta Neuropathol* 2008; 116: 215–20.
- Jack CR, Petersen RC, Xu YC, Waring SC, O'Brien PC, Tangalos EG, et al. Medial temporal atrophy on MRI in normal aging and very mild Alzheimer's disease. *Neurology* 1997; 49: 786–94.
- James BD, Wilson RS, Boyle PA, Trojanowski JQ, Bennett DA, Schneider JA. TDP-43 stage, mixed pathologies, and clinical Alzheimer's-type dementia. *Brain* 2016; 139: 2983–93.
- Josephs KA, Mackenzie I, Frosch MP, Bigio EH, Neumann M, Arai T, et al. LATE to the PART-y. *Brain* 2019a; 142: e47.
- Josephs KA, Dickson DW, Tosakulwong N, Weigand SD, Murray ME, Petrucelli L, et al. Rates of hippocampal atrophy and presence of post-mortem TDP-43 in patients with Alzheimer's disease: a longitudinal retrospective study. *Lancet Neurol* 2017a; 16: 917–24.
- Josephs KA, Murray ME, Tosakulwong N, Weigand SD, Knopman DS, Petersen RC, et al. Brain atrophy in primary age-related tauopathy is linked to transactive response DNA-binding protein of 43 kDa. *Alzheimers Dement* 2019b; 15: 799–806.
- Josephs KA, Murray ME, Tosakulwong N, Weigand SD, Serie AM, Perkerson RB, et al. Pathological, imaging and genetic characteristics support the existence of distinct TDP-43 types in non-FTLD brains. *Acta Neuropathol* 2019c; 137: 227–38.
- Josephs KA, Murray ME, Tosakulwong N, Whitwell JL, Knopman DS, Machulda MM, et al. Tau aggregation influences cognition and hippocampal atrophy in the absence of beta-amyloid: a clinico-imaging-pathological study of primary age-related tauopathy (PART). *Acta Neuropathol* 2017b; 133: 705–15.
- Josephs KA, Murray ME, Whitwell JL, Parisi JE, Petrucelli L, Jack CR, et al. Staging TDP-43 pathology in Alzheimer's disease. *Acta Neuropathol* 2014a; 127: 441–50.
- Josephs KA, Murray ME, Whitwell JL, Tosakulwong N, Weigand SD, Petrucelli L, et al. Updated TDP-43 in Alzheimer's disease staging scheme. *Acta Neuropathol* 2016; 131: 571–85.
- Josephs KA, Whitwell JL, Knopman DS, Hu WT, Stroth DA, Baker M, et al. Abnormal TDP-43 immunoreactivity in AD modifies clinico-pathologic and radiologic phenotype. *Neurology* 2008a; 70: 1850–7.
- Josephs KA, Whitwell JL, Parisi JE, Knopman DS, Boeve BF, Geda YE, et al. Argyliphilic grains: a distinct disease or an additive pathology? *Neurobiol Aging* 2008b; 29: 566–73.
- Josephs KA, Whitwell JL, Tosakulwong N, Weigand SD, Murray ME, Liesinger AM, et al. TAR DNA-binding protein 43 and pathological subtype of Alzheimer's disease impact clinical features. *Ann Neurol* 2015; 78: 697–709.
- Josephs KA, Whitwell JL, Weigand SD, Murray ME, Tosakulwong N, Liesinger AM, et al. TDP-43 is a key player in the clinical features associated with Alzheimer's disease. *Acta Neuropathol* 2014b; 127: 811–24.
- Jovicich J, Czanner S, Greve D, Haley E, van der Kouwe A, Gollub R, et al. Reliability in multi-site structural MRI studies: effects of gradient non-linearity correction on phantom and human data. *NeuroImage* 2006; 30: 436–43.
- Kotrotsou A, Schneider JA, Bennett DA, Leurgans SE, Dawe RJ, Boyle PA, et al. Neuropathologic correlates of regional brain volumes in a community cohort of older adults. *Neurobiol Aging* 2015; 36: 2798–805.
- Kovacs GG, Milenkovic I, Wöhrer A, Höftberger R, Gelpi E, Haberler C, et al. Non-Alzheimer neurodegenerative pathologies and their combinations are more frequent than commonly believed in the elderly brain: a community-based autopsy series. *Acta Neuropathol* 2013; 126: 365–84.
- La Joie R, Perrotin A, Barré L, Hommet C, Mézenge F, Ibazizene M, et al. Region-specific hierarchy between atrophy, hypometabolism, and  $\beta$ -amyloid ( $A\beta$ ) load in Alzheimer's disease dementia. *J Neurosci* 2012; 32: 16265–73.
- Maechler M, Rousseeuw P, Croux C, Todorov V, Ruckstuhl A, Salibián-Barrera M, et al. *robustbase: Basic Robust Statistics*; 2018. Available at: <https://CRAN.R-project.org/package=robustbase>.
- Makinejad N, Schneider JA, Yu J, Leurgans SE, Kotrotsou A, Evia AM, et al. Associations of amygdala volume and shape with transactive response DNA-binding protein 43 (TDP-43) pathology in a community cohort of older adults. *Neurobiol Aging* 2019; 77: 104–11.
- Marino VD, Etienne Y, Niddam M. *The Amygdaloid Nuclear Complex: Anatomic Study of the Human Amygdala*. Springer International Publishing; 2016. Available at: [www.springer.com/gb/book/9783319232423](http://www.springer.com/gb/book/9783319232423) (accessed January 2019).
- McAleese KE, Walker L, Erskine D, Thomas AJ, McKeith IG, Attems J. TDP-43 pathology in Alzheimer's disease, dementia with Lewy bodies and ageing. *Brain Pathol* 2017; 27: 472–9.
- Meyer D, Dimitriadou E, Hornik K, Weingessel A, Leisch F. e1071: Misc Functions of the Department of Statistics, Probability Theory Group (Formerly: E1071). TU Wien; 2018. Available at: <https://CRAN.R-project.org/package=e1071> (accessed December 2018).
- Mirra SS, Heyman A, McKeel D, Sumi SM, Crain BJ, Brownlee LM, et al. The consortium to establish a registry for Alzheimer's disease (CERAD). Part II. Standardization of the neuropathologic assessment of Alzheimer's disease. *Neurology* 1991; 41: 479–86.
- Montine TJ, Phelps CH, Beach TG, Bigio EH, Cairns NJ, Dickson DW, et al. National Institute on Aging-Alzheimer's Association guidelines for the neuropathologic assessment of Alzheimer's disease: a practical approach. *Acta Neuropathol* 2012; 123: 1–11.
- Nag S, Yu L, Boyle PA, Leurgans SE, Bennett DA, Schneider JA. TDP-43 pathology in anterior temporal pole cortex in aging and Alzheimer's disease. *Acta Neuropathol Commun* 2018; 6: 33.

- Nag S, Yu L, Capuano AW, Wilson RS, Leurgans SE, Bennett DA, et al. Hippocampal sclerosis and TDP-43 pathology in aging and Alzheimer disease. *Ann Neurol* 2015; 77: 942–52.
- Nakashima-Yasuda H, Uryu K, Robinson J, Xie SX, Hurtig H, Duda JE, et al. Co-morbidity of TDP-43 proteinopathy in Lewy body related diseases. *Acta Neuropathol* 2007; 114: 221–9.
- Nascimento C, Di Lorenzo Alho AT, Bazan Conceição Amaral C, Leite REP, Nitrini R, Jacob-Filho W, et al. Prevalence of transactive response DNA-binding protein 43 (TDP-43) proteinopathy in cognitively normal older adults: systematic review and meta-analysis. *Neuropathol Appl Neurobiol* 2018; 44: 286–97.
- Nelson PT, Abner EL, Patel E, Anderson S, Wilcock DM, Kryscio RJ, et al. The amygdala as a locus of pathologic misfolding in neurodegenerative diseases. *J Neuropathol Exp Neurol* 2018; 77: 2–20.
- Nelson PT, Dickson DW, Trojanowski JQ, Jack CR, Boyle PA, Arfanakis K, et al. Limbic-predominant age-related TDP-43 encephalopathy (LATE): consensus working group report. *Brain* 2019; 142: 1503–27.
- Nelson PT, Trojanowski JQ, Abner EL, Al-Janabi OM, Jicha GA, Schmitt FA, et al. ‘New old pathologies’: AD, PART, and cerebral age-related TDP-43 with sclerosis (CARTS). *J Neuropathol Exp Neurol* 2016; 75: 482–98.
- Neumann M, Sampathu DM, Kwong LK, Truax AC, Micsenyi MC, Chou TT, et al. Ubiquitinated TDP-43 in frontotemporal lobar degeneration and amyotrophic lateral sclerosis. *Science* 2006; 314: 130–3.
- Olson IR, Plotzker A, Ezzyat Y. The enigmatic temporal pole: a review of findings on social and emotional processing. *Brain* 2007; 130: 1718–31.
- Ossenkoppele R, Pijnenburg YAL, Perry DC, Cohn-Sheehy BI, Scheltens NME, Vogel JW, et al. The behavioural/dysexecutive variant of Alzheimer’s disease: clinical, neuroimaging and pathological features. *Brain* 2015; 138: 2732–49.
- Perry DC, Brown JA, Possin KL, Datta S, Trujillo A, Radke A, et al. Clinicopathological correlations in behavioural variant frontotemporal dementia. *Brain* 2017; 140: 3329–45.
- R Core Team. R: A Language and Environment for Statistical Computing. Vienna: R Foundation for Statistical Computing; 2014. Available at: <http://www.R-project.org/>.
- Roberts RO, Geda YE, Knopman DS, Cha RH, Pankratz VS, Boeve BF, et al. The Mayo Clinic study of aging: design and sampling, participation, baseline measures and sample characteristics. *Neuroepidemiology* 2008; 30: 58–69.
- Schwarz CG, Gunter JL, Ward CP, Vemuri P, Senjem ML, Wiste HJ, et al. The Mayo Clinic adult life span template: better quantification across the life span. *Alzheimer’s Dement* 2017; 13: P93–4.
- Tan RH, Kril JJ, Fatima M, McGeachie A, McCann H, Shepherd C, et al. TDP-43 proteinopathies: pathological identification of brain regions differentiating clinical phenotypes. *Brain* 2015; 138: 3110–22.
- Wennerg AM, Tosakulwong N, Lesnick TG, Murray ME, Whitwell JL, Liesinger AM, et al. Association of apolipoprotein E  $\epsilon$ 4 with transactive response DNA-binding protein 43. *JAMA Neurol* 2018; 75: 1347–54.
- Wennerg AM, Whitwell JL, Tosakulwong N, Weigand SD, Murray ME, Machulda MM, et al. The influence of tau, amyloid, alpha-synuclein, TDP-43, and vascular pathology in clinically normal elderly individuals. *Neurobiol Aging* 2019; 77: 26–36.
- Whitcher V, Schmid VJ, Thornton A. Working with the DICOM and NIFTI data standards in R. *J Stat Softw* 2011; 440: 1–28.
- Whitwell JL, Josephs KA, Murray ME, Kantarci K, Przybelski SA, Weigand SD, et al. MRI correlates of neurofibrillary tangle pathology at autopsy: a voxel-based morphometry study. *Neurology* 2008; 71: 743–9.
- Yang H-S, Yu L, White CC, Chibnik LB, Chhatwal JP, Sperling RA, et al. Evaluation of TDP-43 proteinopathy and hippocampal sclerosis in relation to APOE  $\epsilon$ 4 haplotype status: a community-based cohort study. *Lancet Neurol* 2018; 17: 773–81.
- Yokota O, Davidson Y, Arai T, Hasegawa M, Akiyama H, Ishizu H, et al. Effect of topographical distribution of  $\alpha$ -synuclein pathology on TDP-43 accumulation in Lewy body disease. *Acta Neuropathol* 2010; 120: 789–801.
- Zhang X, Sun B, Wang X, Lu H, Shao F, Rozemuller AJM, et al. Phosphorylated TDP-43 staging of primary age-related tauopathy. *Neurosci Bull* 2019; 35: 183–92.
- Zhang J, Zhang Y, Xing S, Liang Z, Zeng J. Secondary neurodegeneration in remote regions after focal cerebral infarction: a new target for stroke management? *Stroke* 2012; 43: 1700–5.